Percolation and clustering in supercritical aqueous fluids

2008 J. Phys.: Condens. Matter 20 494208

(http://iopscience.iop.org/0953-8984/20/49/494208)

J. Phys.: Condens. Matter **20** (2008) 494208 (8pp) doi:10.1088/0953-8984/20/49/494208

Percolation and clustering in supercritical aqueous fluids

M Bernabei[1,2] **and M A Ricci**[1]

[1] Dipartimento di Fisica 'E Amaldi', Università degli Studi 'Roma Tre', Via della Vasca Navale 84, 00146 Roma, Italy
[2] Donostia International Physics Center, Paseo Manuel de Lardizabal 4, 20018 San Sebastian, Spain

Received 22 July 2008, in final form 2 September 2008
Published 12 November 2008
Online at stacks.iop.org/JPhysCM/20/494208

Abstract

Neutron diffraction data for pure supercritical water and supercritical mixtures of water and CO_2 are analyzed by using the empirical potential structure refinement Monte Carlo simulation, and molecular configurations compatible with the experimental data are recorded. The analysis of the distribution functions of water cluster size in these fluids allows the identification of a percolation line, which separates gas-like states from liquid-like ones, in pure supercritical water. Solvation of CO_2 in supercritical water inhibits cluster percolation, although the radial distribution functions show liquid-like behavior: this is likely to be due to the excess volume being localized around the CO_2 molecules.

(Some figures in this article are in colour only in the electronic version)

1. Introduction

Supercritical aqueous fluids are important media for new greenhouse chemistry and geological research [1–8]. The peculiar properties of supercritical water as a solvent, and in particular the tunable solubility of minerals and aromatic complexes in supercritical water or in mixtures of water and CO_2, have great relevance for their industrial applications and fundamental research in geology. Pressure changes at constant temperature may indeed enable selective precipitation of solutes, and understanding this mechanism can elucidate the origin of rocks under the Earth's mantle and suggests new technology for waste treatment. Such interesting behavior has stimulated several studies of both the structure and dynamics of supercritical water [9–31] and water–CO_2 mixtures [2, 32–36]. Here we will limit our attention to studies of the microscopic structure of both pure supercritical water [9–13, 15–18, 26–31] and its mixtures with CO_2 [2, 32–34]. These have been performed by using neutron or x-ray diffraction and molecular dynamics simulations, and most of them are relative to high density states. The first experiments [31] and simulations [29, 30] on low density supercritical water have appeared only quite recently. All studies show strong differences between the water–water radial distribution functions (RDF) at supercritical states compared to ambient ones. In particular, both the first and second peaks of the $g_{\mathrm{OwOw}}(r)$ function move to larger distances, and more importantly the ratio between the position of the first and second peaks increases from ∼1.6 to ∼2, suggesting that the extended almost tetrahedral network of hydrogen bonds (HB) characteristic of ambient water is largely disrupted at supercritical conditions. Nevertheless the $g_{\mathrm{OwHw}}(r)$ function exhibits the signature of intermolecular HB, that is a peak or a shoulder at $r \sim 0.9$ Å, also above the critical temperature, although the number of HB per molecule is confirmed to be strongly reduced. The presence of a residual HB peak in the RDF of supercritical water, also at the lowest densities investigated, has suggested that an analysis of the water configurations in terms of percolation theory may be feasible and permit the definition of a percolation line, separating percolating states from non-percolating ones, in the supercritical region of the Clapeyron plane [29, 30]. We have recently shown that neutron diffraction data for pure supercritical water confirm these molecular dynamics (MD) results [31], and we will review those findings here, along with a percolation analysis of a neutron diffraction experiment performed in a supercritical mixture of water and CO_2 [33, 34]. This will allow us to demonstrate important structural differences between percolating and non-percolating states of pure water and to make inferences about the structural origin of the excess volume in the water–CO_2 mixtures.

Neutron diffraction is a powerful technique for experimental investigation of the microscopic structure of molecular

liquids, since isotopic labeling of the individual nuclei gives access to distinct differential cross sections for the 'same' fluid [34]. In the classical approximation we can indeed assume that isotopic substitution does not affect the microscopic structure of the fluid, but simply changes the contrast of the substituted nuclei with respect to the others, during the interaction with the neutrons, by changing their neutron scattering length, b, in the Fermi effective potential [37]. Provided that isotopes are available for a sufficient number of atomic species, the measured cross sections can be decomposed into atom–atom RDF, with a clear advantage with respect to x-ray diffraction experiments. In the case of pure water, the H/D substitution allows us to extract all three RDF: $b_{\mathrm{H}} = -3.742$ fm and $b_{\mathrm{D}} = 6.674$ fm [37]. Nevertheless these functions depend on the modulus of the distance between the atomic pair, and complete information on the orientational correlations, or on the connectivity of the HB network through the analysis of the cluster size, is not directly accessible but is embedded into the RDF. In order to extract this information from the experiment and reconstruct a three-dimensional model for the liquid, as in any computational work, we need a collection of molecular configurations: these become available when the experimental data are used to constrain a computer simulation. The reliability of this reconstruction will obviously depend on the quality and quantity of the available experimental data along with the quality of their fit through the simulation. In the following we will apply the empirical potential structure refinement (EPSR) method [38–41], based on a Monte Carlo (MC) simulation technique.

2. Formalism and definitions for the percolation analysis

An ensemble of water molecules is said to percolate when the distribution function of the cluster size, n, exceeds the so-called percolation threshold, $P(n)$, defined as:

$$P(n) \sim n^{-\tau} \tag{1}$$

with the universal exponent $\tau = 2.19$ in three-dimensional systems [42, 43]. It can be demonstrated that this condition is satisfied as soon as the average number of HB per molecule exceeds the critical value of 1.55 [44]. In bulk ambient or supercooled water this condition is fully verified and the fluid can be described as a percolating HB network, which continuously reconstructs itself on the picosecond lifetime of the HB [45–47].

In order to evaluate the dimensions of the HB clusters within a water sample and their distribution function, a definition of the HB pair and cluster is needed. Since our configurations are derived from the diffraction experiment using a MC code, only a geometrical criterion can be used for these definitions. In particular we consider two water molecules to be H-bonded when the distance of a proton on one molecule to the oxygen of the second is less than or equal to the position of the first minimum of the $g_{\mathrm{OH}}(r)$ at ambient conditions (i.e. 2.4 Å). Moreover a group of molecules forms a cluster if each pair of molecules is bonded to at least one other molecule in the cluster. It has to be mentioned that although more complex definitions of a HB pair could be adopted, accounting for instance also for the $\hat{\mathrm{OHO}}$ angle, nevertheless the overall picture of the system does not change and our choice is the less demanding in terms of computational time.

We notice that although the concept of percolation implies in principle the formation of an infinite cluster, which may only occur in an infinite system, equation (1) also defines a percolation threshold in a finite system, such as a simulation box. Within a MC simulation it is then expected that a system of molecules at the percolation threshold exhibits a distribution of cluster sizes close to the power law defined in equation (1), which will be a straight line on a log–log scale. If the system is below the percolation threshold, its distribution function will deviate from the straight line and decreases more rapidly with increasing cluster size. For systems above the threshold it is instead expected that the distribution of clusters exceeds the threshold value at sufficiently large size. Systems well above the threshold show a peak at about the size of the ensemble of molecules, due to the presence of clusters spanning the entire simulation box. However, due to the finite size of the box, the intensity of this peak increases at the expense of the population of smaller clusters, giving deviations of the distribution functions from a straight line at low and intermediate cluster sizes.

Table 1. Temperature, pressure and density of the investigated states.

Label	T (K)	P (bar)	CO_2 (%)	ρ (kg m^{-3})
A	673	250	0	116
B*	673	500	0	580
B	673	1500	0	750
C[1]	673	1300	0.92	463
C[10]	673	1300	9.2	559

3. Experimental methods and data analysis

All the experiments reported here have been performed at $T = 673$ K, at pressures between 250 and 1500 bar and densities ranging from 0.0116 to 0.0753 atoms Å^{-3} (see table 1), the critical density of water being $\rho_c = 0.0322$ atoms Å^{-3} [48]. Data for the water–CO_2 mixture have been measured at constant pressure, $P = 1300$ bar, at two CO_2 molar fractions, namely 0.92% and 9.2%. These states correspond to a number density of the mixtures equal to 0.0458 and 0.049 atoms Å^{-3}, respectively, i.e. lower than that of water at the same temperature and pressure, due to volume excess upon CO_2 solvation (see figure 1) [2, 49]. For the forthcoming discussion it is useful to notice here that the volume excess is higher at the lowest CO_2 molar fraction. Details about the sample container and sample preparation may be found in [31] and [33], respectively.

Neutron diffraction measurements were performed on the SANDALS [50] diffractometer, installed at the ISIS facility (UK) [51]. Temperature control was achieved by heaters in contact with the top and bottom of the sample container, giving a temperature stability better than ±0.1 K. The isotopic H/D substitution [34] has been applied and data have been collected

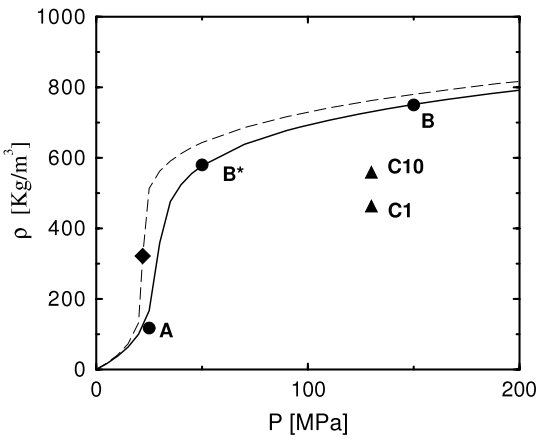

Figure 1. Critical isotherm (dashed line) and critical point (solid diamond) of pure water, along with the experimental points (solid circle) along the isotherm $T = 673$ K. The ρ, P values corresponding to the two water–CO_2 mixtures are reported as solid triangles, for comparison: notice the largest excess volume at the lowest CO_2 molar fraction.

on a fully deuterated sample, a fully hydrogenated one and a 50% mixture of the two (hereafter labeled HDO), in order to maximize the contrast between the three experimental data. At state point A only the fully deuterated and the H/D equimolar mixture were measured, since the signal to noise ratio for the fully hydrogenated sample was prohibitive. Data at different state points have been measured at distance of several months or years, and their internal consistency is a benchmark of their quality.

Data reduction was performed using the Gudrun routine available on SANDALS, which performs corrections for multiple scattering, absorption and inelasticity effects, along with subtraction of the scattering from the sample container, and data reduction to an absolute scale, following the procedure described in the ATLAS manual [52]. The output of the Gudrun routine is the interference differential cross sections (IDCS), $F(Q)$, defined in equations (2)–(4) and measured in barn/atom sr:

$$F(Q) = \Sigma_\alpha \Sigma_{\beta \geqslant \alpha} w_{\alpha\beta}[S_{\alpha\beta}(Q) - 1] \tag{2}$$

where Q, the momentum transferred in the interaction between a neutron and a nucleus, is defined as a function of the neutron wavelength, λ, and scattering angle, 2θ by

$$Q = \frac{4\pi}{\lambda} \sin\,\theta \tag{3}$$

and the weighting factors

$$w_{\alpha\beta} = c_\alpha c_\beta b_\alpha b_\beta (2 - \delta_{\alpha\beta}) \tag{4}$$

depend on the neutron scattering lengths, b_α and b_β [37], of the $\alpha\beta$ atom pairs, while the Kronecker $\delta_{\alpha\beta}$ avoids double counting of like terms in the summation. The $S_{\alpha\beta}(Q)$ are called partial structure factors (PSF) and are defined as Fourier transforms of the corresponding RDF of the $\alpha\beta$ pair, $g_{\alpha\beta}(r)$:

$$(S_{\alpha\beta}(Q) - 1) = 4\pi\rho \int_0^\infty r^2 (g_{\alpha\beta}(r) - 1) \frac{\sin(Qr)}{Qr}\,\mathrm{d}r. \tag{5}$$

With the hypothesis that the microscopic structure of the deuterated sample does not sensibly differ from that of the hydrogenated one, the difference between the three IDCS depends only on the different weighting factors. In the case of pure water, three RDF of interest, namely $g_{\mathrm{OwOw}}(r)$, $g_{\mathrm{OwH}}(r)$ and $g_{\mathrm{HH}}(r)$, can readily be extracted from the experimental data. Instead, in the case of the water–CO_2 mixtures the 10 individual partial RDF cannot be extracted from the three IDCS, without the support of a computer simulation, for instance the EPSR routine [38–41]. Moreover it has to be borne in mind that given the relative weights of the individual PSF, the water–water and solute–solute correlations will be the best and the worst determined respectively.

The EPSR is a Monte Carlo routine, which builds up a three-dimensional model of the sample that is constrained by the available independent experimental data sets (the IDCS in this case). The routine requires as input the sample composition and thermodynamic parameters and a model for the site–site interactions, which will be used as 'reference' to start and equilibrate the simulation. This model needs to incorporate the characteristics of the sample, such as the correct molecular geometry and, in the case of aqueous fluids, the effective point charges, in order to emulate the H-bonding between water molecules. Among the many available models, in the present case we have used the simple point charge/extended (SPC/E) [53] model for water and the elementary physical model-modified (EPM-M) [54] model for the interaction between CO_2 molecules. Both models consist of a Lennard-Jones contribution plus Coulombic interactions between charged sites and the Lorentz–Berthelot rules have been applied in order to evaluate the interaction between different atomic species. The simulations have been performed in the NVE ensemble by applying periodic boundary conditions and setting a potential cut-off to 12 Å. After equilibration, an empirical correction to the reference potential has been evaluated iteratively within the routine, in order to achieve the best fit to the experimental $F(Q)$ functions. This iterative procedure leads to the refinement of the so-called 'empirical potential', which is used while accumulating molecular configurations, during the production run. This technique enables the noise in the radial distribution functions to be reduced to an insignificant level, avoiding the direct Fourier transform of the experimental data. Moreover, the availability of molecular configurations allows us to access other structural quantities not otherwise available from the experiment, like for instance the cluster size distribution discussed in this paper. The typical quality of an EPSR fit to the NDIS data is shown in figure 2, where the data relative to state point B^* are reported as an example. The typical shape, intensity and r-range of the 'empirical' potential can be appreciated by looking at figure 3, where this is compared with the SPC/E contribution for the interaction between water oxygens, in the case of state points C1 and C10.

4. Radial distribution functions

The water–water RDF, reported in figures 4–6, clearly show that the microscopic structure of supercritical water at state point A is gas-like, with all three RDF slowly decaying to

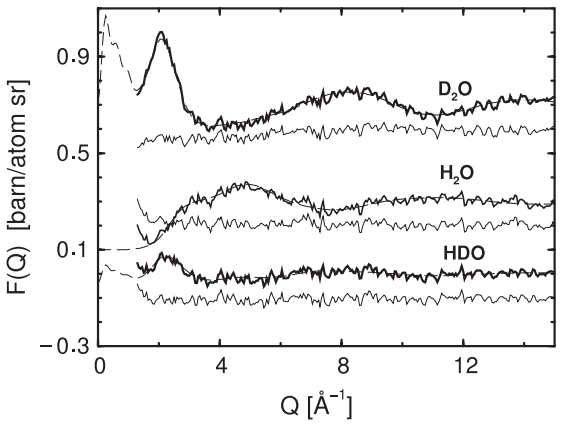

Figure 2. Experimental IDCS (thick solid line) along with their EPSR fit (dashed line) for the three pure water samples measured at state point B*. The fit residuals are reported as thin solid lines (down-shifted) to show the substantial absence of residual structures. Data for HDO and D_2O have been arbitrarily shifted for clarity.

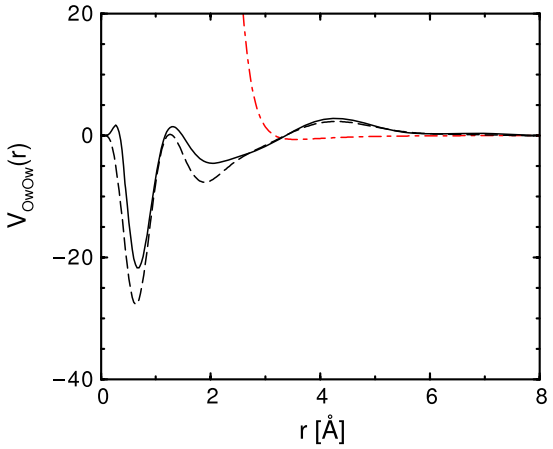

Figure 3. The interaction potential between water oxygens: the red dot-dashed line represents the 'reference' potential; the 'empirical potential' for the 0.92% CO_2 solution (state point C1) and the 9.2% one (state point C10) are reported as a black solid and black dashed lines respectively.

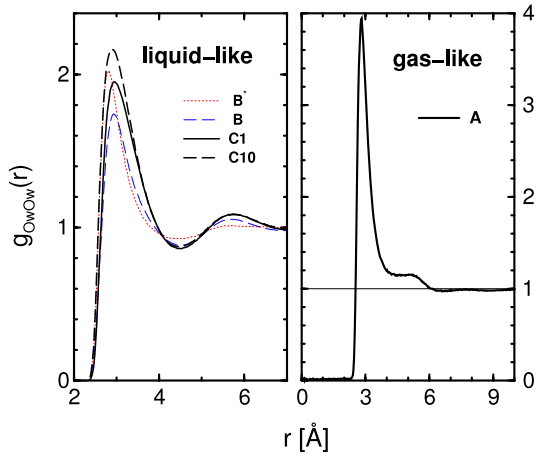

Figure 4. Comparison between the $g_{OwOw}(r)$ functions obtained at state point A (right panel) and (in the left panel) at states B* (red dotted), B (blue dot-dashed), C1 (black solid), C10 (black dashed). Notice that the scale of the ordinate for the gas-like state is reported on the right axis.

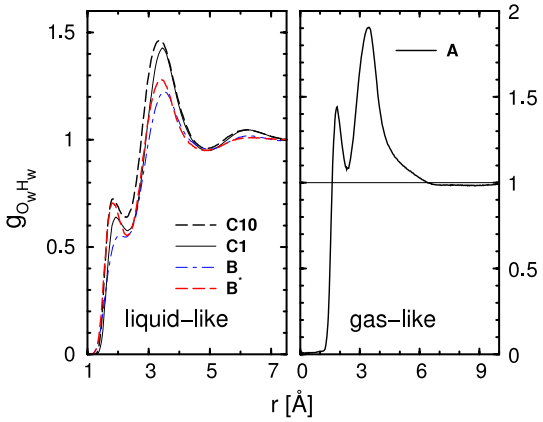

Figure 5. Comparison between the $g_{OwHw}(r)$ functions obtained at state point A (right panel) and (in the left panel) at states B* (red dotted), B (blue dot-dashed), C1 (black solid), C10 (black dashed). Notice that the scale of the ordinate for the gas-like state is reported on the right axis.

their asymptotic value, without oscillations about 1, while at all other states it is liquid-like. Among the liquid-like functions there are small differences, showing a dependence on pressure or CO_2 content, which have already been discussed in detail in [31, 33, 34]. Here we recall that all these RDF show the characteristic features of supercritical water, and in particular that the second peak of the $g_{OwOw}(r)$ is centered between 5.6 and 5.85 Å, that is at about twice the position of the first peak, while in ambient water this peak is centered at 4.5 Å and is considered the signature of the extended tetrahedral network of HB. We notice also that the effect of CO_2 solvation is a broadening of the main peaks of the RDF and an enhancement of their oscillations. The latter feature has been considered to be a signature of enhanced clustering in previous MD simulations [2].

In order to perform an analysis of the molecular configurations in terms of percolation and clustering, the presence at all investigated states of a well resolved peak at ∼1.9 Å is relevant; that is the signature of the presence of HB also at supercritical states.

Among the other RDF available in the case of water–CO_2 mixtures, we report here only the $g_{OwO}(r)$, shown in figure 7 in comparison with the $g_{OwOw}(r)$ functions, and observe that both the minimum approach distance and the position of the first peak of the $g_{OwOw}(r)$ functions are shorter that those of the $g_{OwO}(r)$ ones.

Finally we want to mention an important difference between the microscopic structure of gas-like and liquid-like supercritical aqueous fluids which is not directly visible in the RDF. This is the three-dimensional organization of water molecules around a water molecule of given orientation that can be visualized by developing the RDF into their spherical harmonic components and computing the spatial density functions (SDF), following the seminal work of

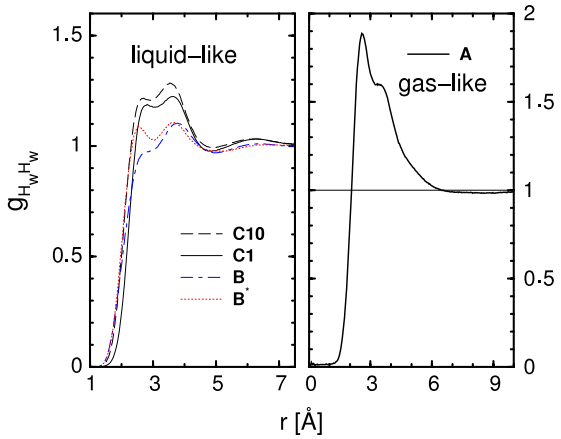

Figure 6. Comparison between the $g_{\mathrm{HwHw}}(r)$ functions obtained at state point A (right panel) and (in the left panel) at states B* (red dotted), B (blue dot-dashed), C1 (black solid), C10 (black dashed). Notice that the scale of the ordinate for the gas-like state is reported on the right axis.

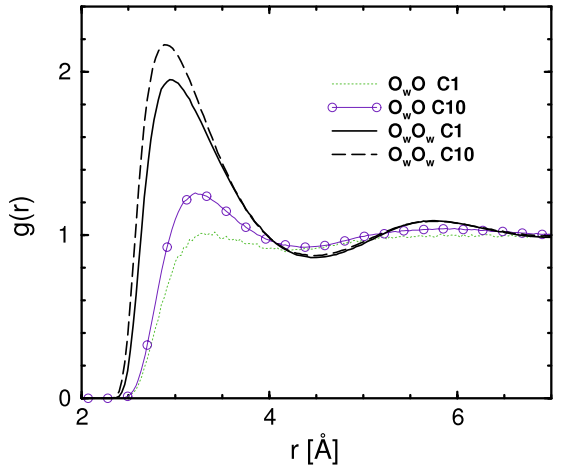

Figure 7. Comparison between the RDF of water oxygens in the two supercritical mixtures investigated (black solid and dashed lines as in figure 4) and the RDF of water oxygens and CO_2 oxygens. Data relative to state C1 are reported as a green dotted line and those relative to state C10 as an indigo solid line with circles.

Svishchev and Kusalik [55]. The SDF identify, around a central molecule, the regions where the probability of finding another molecule, averaged over orientations, exceeds a threshold value. In [31] (see figure 10) we have shown that in the case of pure supercritical water the isosurfaces of probability relative to molecules in the first and second shell have the same spatial symmetry, contrary to what happens at ambient conditions [55]. Interestingly the SDF at state point A exhibits a triangular symmetry instead of a tetrahedral one, characteristic of water at ambient conditions as well as at supercritical liquid-like ones. When the probability threshold is lowered (contrast increased) the first neighbor shell is isotropically occupied at all investigated supercritical states and an almost perfect spherical symmetry is recovered at the highest density states. We stress that the triangular symmetry of the SDF functions at state point A implies that

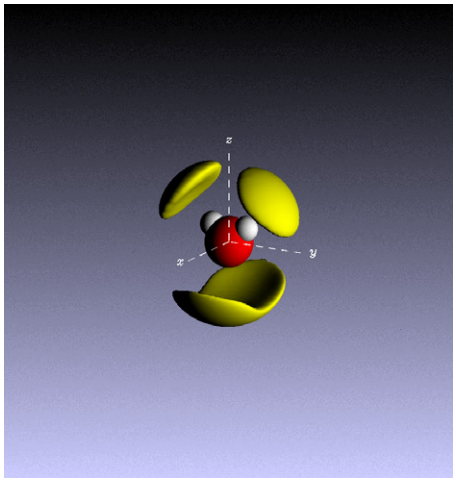

Figure 8. Spatial density functions for water molecules around a central water molecule, calculated at state point C1, with a contrast level equal to 0.25 and including only water molecules within the first neighbor shell. Note the tetrahedral symmetry of this shell at this contrast level.

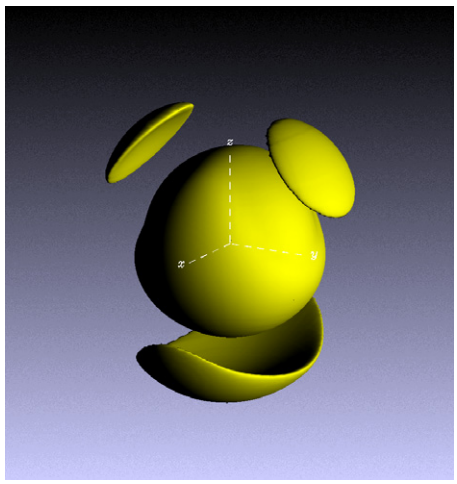

Figure 9. Spatial density functions for water molecules around a central water molecule, calculated at state point C1, with a contrast level equal to 0.25 and including water molecules belonging to the first and second neighbor shells. Note that as in liquid-like states of pure supercritical water, the first shell is here almost spherical and the second has the same tetrahedral symmetry as the first shell of figure 8.

water molecules are organized in small chains or sheets, while at the other states three-dimensional network-like clusters may grow up. Here we report the SDF for water in the supercritical C1 mixture (see figures 8 and 9): these show the same characteristics found for liquid-like states in pure supercritical water. The SDF at state point C10 are almost identical to those reported here.

5. Percolation and clustering

In figures 10 and 11 we report the distribution functions of the fraction, $F(i_{\text{H-bond}})$, of water molecules engaged in i HB at all

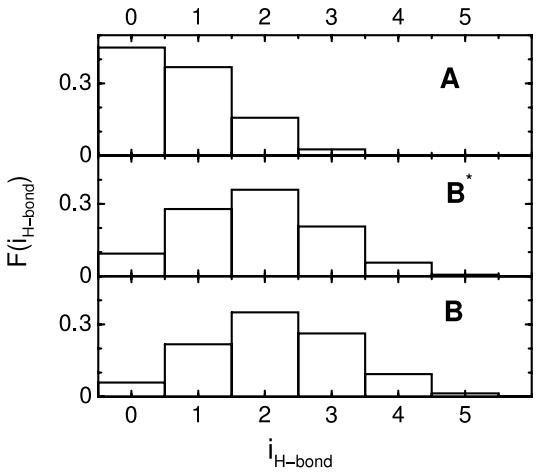

Figure 10. The distribution function of molecules with i HB, in the case of pure supercritical water, giving an average number of HB per molecule equal to 0.8 for gas-like water, compared with ∼2 for liquid-like supercritical water.

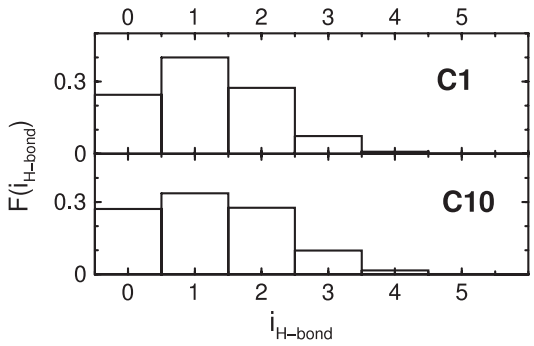

Figure 11. The distribution function of molecules with i HB, in the case of supercritical water–CO_2 mixtures, giving an average number of HB per molecule of the order of 1.2, that is below the percolation threshold value.

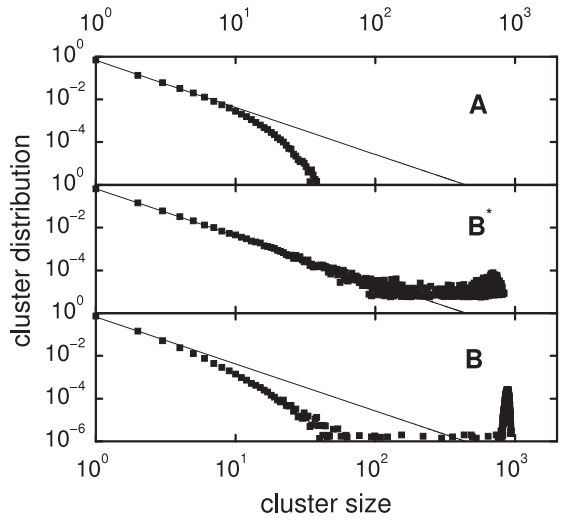

Figure 12. The distribution function of the size of HB clusters, for supercritical water at states A, B* and B (solid squares), compared with the distribution function for a system at the percolation threshold (solid line). Both states B* and B are above the percolation threshold, although finite size effects are visible in the simulation relative to the higher density state.

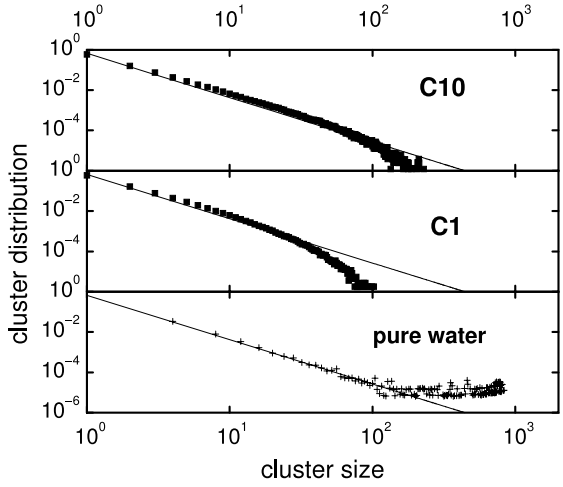

Figure 13. The distribution function of the size of HB clusters, for supercritical water–CO_2 mixtures at states C1, and C10 (solid squares), compared with the distribution function for a system at the percolation threshold (solid line). The crosses in the bottom panel are the results obtained in a simulation of pure supercritical water at the same density as mixture C1, showing that the presence of CO_2, not the density, inhibits percolation in the mixtures.

investigated states. The average number of HB per molecule is above the percolation threshold at liquid-like supercritical states in pure water, being 1.9 and 2.2 at states B* and B, respectively. It is instead below the threshold at state point A (0.8) and in the water–CO_2 mixtures (∼1.2). Assuming that $F(i_{\text{H-bond}})$ is binomial, the probability that a HB is intact can be evaluated as $p_B = F(4)^{0.25}$ [44, 46, 47]. This simple calculation gives $p_B = 0.214$ at state point A, $p_B = 0.488$ and 0.555 at states B and B*; $p_B = 0.305$ and $p_B = 0.360$ for the supercritical mixtures C1 and C10, respectively. According to these findings, percolating water clusters should be present in samples B and B* and absent in the other cases, 0.4 being the threshold value of p_B for percolating systems.

The distribution function of the cluster size at all state points investigated is reported in figures 12 and 13, along with the threshold distribution $P(n)$ (solid line). As far as the pure water states are concerned, we notice that state B* seems to be just about the percolation threshold, while state A is clearly below and state B above. In the latter case the experimental distribution exceeds the threshold value at $n \sim 350$ and has a pronounced maximum at $n \sim 900$ molecules; finite size effects are visible in the range $30 \leqslant n \leqslant 140$. These findings are in agreement with the simulations reported in [29] at similar thermodynamic states, and demonstrate that in supercritical water a percolation line can be defined as the locus of thermodynamic states which separates liquid-like from gas-like structures.

Both investigated supercritical mixtures stay instead below the percolation threshold, although their RDF show liquid-like behavior. This could be in principle a trivial consequence of the excess volume, which implies a lower density of the water–CO_2 mixture compared to pure

supercritical water at the same temperature and pressure. We then performed a simulation run of pure supercritical water at a density of 0.046 atoms $Å^{-3}$, by using the 'empirical potential' refined within the EPSR simulation of supercritical water at $T = 673$ K and $P = 500$ bar and evaluated the cluster distribution in this case (also reported in figure 13). This simulation demonstrated that pure water at such a low density is still above the percolation threshold and consequently the absence of percolation in the mixtures is not a trivial consequence of the volume excess of the mixture. The evidence that both minimum approach and average distance of the O_w–O pairs are larger than the O_w–O_w ones (see figure 7) suggests instead that the excess volume is localized around the CO_2 solute. The presence of the solute limits the size of the water clusters due to a sort of excluded volume effect, and the deviation of the cluster size distribution function from the threshold value is larger for the most diluted mixture, that also shows the largest excess volume (see figure 1). Incidentally our findings demonstrate that the enhanced oscillations of the RDF with respect to pure water cannot be ascribed to enhanced clustering, as suggested in [2].

6. Conclusions

By analyzing neutron diffraction data through the EPSR code, we have shown that in the case of pure supercritical water a percolation line separates two structurally different fluids as the density decreases from values typical of a so-called liquid-like fluid to those of a gas-like system. It appears indeed that water even above its supercritical temperature can be considered as a highly dynamic percolating system, provided that the density is high enough for the RDF to show the oscillatory character typical of liquid-like systems. At low densities, when the RDF show gas-like behavior, water does not percolate. The transition is marked by a percolation line. Interestingly the observation that this line separates gas-like from liquid-like states may also suggest a possible relation with the Fisher–Widom line [56, 57], defined for simple liquids. To our knowledge this relation has been investigated or proposed and perhaps this issue merits further checks in other pure systems, although its validity looks questionable in fluid mixtures, like for instance water–CO_2. More importantly, the transition through the percolation line is accompanied by clear changes in the three-dimensional structure of the fluid. In particular the preferred tetrahedral arrangement of first neighboring molecules persists at liquid-like densities, while a triangular symmetry is found at gas-like states. This is correlated with the average number of HB per molecule, which decreases from ∼2 to ∼0.8 upon the transition: in other words, when the probability of finding a four-bonded molecule is below the threshold value of ∼0.25% (as for instance at state point A), the tetrahedral spatial arrangement becomes unlikely. As a matter of fact the distribution functions reported in figure 10 predict that within an ensemble of 1000 water molecules only two form four HB at state point A, while this number becomes of the order of 50 or 100 for the liquid-like states. Consequently, while liquid-like supercritical water can still be described as a percolating system formed by three-dimensional clusters or branched chains, at gas-like densities water molecules are predominantly isolated or organized in small sheet-like oligomers.

The situation becomes more intriguing when a hydrophobic solute is solvated in supercritical water. Here we have shown that in the case of water–CO_2 mixtures cluster percolation is inhibited, although the RDF behave as liquid-like and the SDF for water molecules around another water molecule have the same symmetry and character as those of pure supercritical water at states B^* and B. We have demonstrated that this is not a trivial effect of the excess volume and is instead due to the nature of the water–CO_2 interaction. The observation that on average the distance between water oxygens is shorter that that between a water oxygen and an oxygen belonging to the CO_2 molecule suggests that the excess volume is probably localized around the CO_2 molecules and that although water molecules are locally organized in liquid-like three-dimensional clusters, these cannot percolate through the simulation box because of the regions occupied by the solute. Moreover, the finding that at state C10 the probability that an HB is intact is higher and the deviations of the distribution of the clusters size from the threshold behavior is reduced compared to state C1, suggests that the absence of percolation in these mixtures is correlated with the excess volume in a non-trivial manner.

Acknowledgments

This work has been performed within the agreement no 01/9001 between CCLRC and CNR concerning collaboration in scientific research at the spallation neutron source ISIS and with partial financial support of CNR.

References

[1] Mather A E and Franck E U 1992 *J. Phys. Chem.* **96** 6
[2] Destrigneville C M, Brodholt J P and Wood B 1996 *J. Chem. Geol.* **133** 53
[3] Modell M 1989 Supercritical water oxidation *Standard Handbook of Harzardous Waste Treatment and Disposal* ed Z H M Freeman (New York: McGraw-Hill)
[4] Macdonald D D and Kriksunov L B 2001 *Electrochim. Acta* **47** 775
[5] DeSimone J M, Zihibin G and Elsbernd C S 1992 *Science* **257** 945
[6] DeSimone J J, Maury E E, Menceloglu Y Z, McClain J N, Romack T J and Combes J R 1994 *Science* **265** 356
[7] McClain J B, Betts D E, Canelas D A, Samulski E T, DeSimone J M, Londono J D, Cochran H D, Wignall G D, Chillura Martino D and Triolo R 1996 *Science* **274** 2049
[8] Papers in Dec. Issue of 2000 *Ind. Eng. Chem. Res.* **39**
[9] Postorino P, Tromp R H, Ricci M A, Soper A K and Neilson G W 1993 *Nature* **366** 668
[10] Postorino P, Ricci M A and Soper A K 1994 *J. Chem. Phys.* **101** 4123
[11] Tromp R H, Postorino P, Neilson G W, Ricci M A and Soper A K 1994 *J. Chem. Phys.* **101** 6210
[12] Soper A K, Bruni F and Ricci M A 1997 *J. Chem. Phys.* **106** 247
[13] Bellissent-Funel M C, Tassaing T, Zhao H, Beysens D, Guillot B and Guissani Y 1997 *J. Chem. Phys.* **107** 2942

[14] Tassaing T, Bellissent-Funel M C, Guillot B and Guissani Y 1998 *Europhys. Lett.* **42** 265
[15] Jedlovsky P, Brodholt J P, Bruni F, Ricci M A, Soper A K and Vallauri R 1998 *J. Chem. Phys.* **108** 8528
[16] Botti A, Bruni F, Ricci M A and Soper A K 1998 *J. Chem. Phys.* **109** 3180
[17] Gorbatyi Yu E and Demianets Yu N 1982 *J. Struct. Chem.* **23** 882
[18] Gorbatyi Yu E and Demianets Yu N 1983 *J. Struct. Chem.* **24** 385
[19] Morita T, Kusano K, Ochiai H, Saitow K and Nishikawa K 2000 *J. Chem. Phys.* **112** 4203
[20] Matubayasi N, Wakai C and Nakahara M 1999 *J. Chem. Phys.* **110** 8000
[21] Matubayasi N, Nakao N and Nakahara M 2001 *J. Chem. Phys.* **114** 4107
[22] Tassaing T and Bellissent-Funel M-C 2000 *J. Chem. Phys.* **113** 3332
[23] Tassaing T, Danten Y and Besnard M 2004 *Pure Appl. Chem.* **76** 133
[24] Andreani C, Colognesi D, Degiorgi E and Ricci M A 2001 *J. Chem. Phys.* **115** 11243
[25] Ricci M A, Nardone M, Fontana A, Andreani C and Hahn W 1998 *J. Chem. Phys.* **108** 450
[26] Fois E S, Sprik M and Parrinello M 1994 *Chem. Phys. Lett.* **223** 41
[27] Boero M, Terakura K, Ikeshoji T, Liew C C and Parrinello M 2001 *J. Chem. Phys.* **115** 2219
[28] Kalinichev A G and Bass J D 1997 *J. Phys. Chem.* **101** 9720
[29] Partay L and Jedlovsky P 2005 *J. Chem. Phys.* **123** 024502
[30] Partay L, Jedlovsky P, Brovchenko I and Oleinikova A 2007 *Phys. Chem. Chem. Phys.* **9** 1341
[31] Bernabei M, Botti A, Bruni F, Ricci M A and Soper A K 2008 *Phys. Rev.* E **78** 021505
[32] Kalinichev A G and Kirkpatrick R J 2001 *11th Annual V M Goldsmidt Conf. 3298.pdf*
[33] Lo Celso F, Triolo R, Ferrante F, Botti A, Bruni F, Mancinelli R, Ricci M A and Soper A K 2007 *J. Mol. Liq.* **136** 294
[34] Botti A, Bruni F, Mancinelli R, Ricci M A, Lo Celso F, Triolo R, Ferrante F and Soper A K 2008 *J. Chem. Phys.* **128** 164504
[35] Oparin R, Tassaing T, Danten Y and Besnard M 2004 *J. Chem. Phys.* **120** 10691
[36] Oparin R, Tassaing T, Danten Y and Besnard M 2005 *J. Chem. Phys.* **123** 224501
[37] Sears V F 1992 *Neutron News* **3** 26
[38] Soper A K 1996 *Chem. Phys.* **202** 295
[39] Soper A K 2000 *Chem. Phys.* **258** 121
[40] Soper A K 2001 *Mol. Phys.* **99** 1503
[41] Bowron D T, Finney J L and Soper A K 1998 *J. Phys. Chem.* B **102** 3551
[42] Stauffer D 1985 *Introduction to Percolation Theory* (London: Taylor and Francis)
[43] Oleinikova A, Brovchenko I, Geiger A and Guillot B 2002 *J. Chem. Phys.* **117** 3296
[44] Blumberg R L, Stanley H E, Geiger A and Mausbach P 1984 *J. Chem. Phys.* **80** 5230
[45] Stanley H E 1979 *J. Phys. A: Math. Gen.* **12** L329
[46] Stanley H E and Teixeira J 1980 *J. Chem. Phys.* **73** 3404
[47] Geiger A and Stanley H E 1982 *Phys. Rev. Lett.* **49** 1895
[48] Nist Chemistry Webbook www.webbook.nist.gov
[49] Seitz J C and Blencoe J G 1999 *Geochim. Cosmochim. Acta* **63** 1559
[50] Soper A K 1989 *Proc. Conf. on Advanced Neutron Sources 1988* (*IOP Conf. Proc.* no. 97) ed D K Hyer (London: Institute of Physics and Physical Society) pp 353–66
[51] www.isis.rl.ac.uk
[52] www.isis.rl.ac.uk/disordered/Sandals/ATLASmanualDTB.pdf
[53] Berendsen H J C, Grigera J R and Straatsma T P 1987 *J. Phys. Chem.* **91** 6269
[54] Harris J and Young K H 1995 *J. Phys. Chem.* **99** 12021
Zhang Y, Yang J and Yu Y-X 2005 *J. Phys. Chem.* B **109** 13375
[55] Svishchev I M and Kusalik P G 1993 *J. Chem. Phys.* **99** 3049
[56] Fisher M E and Widom B 1969 *J. Chem. Phys.* **50** 3756
[57] Leote de Carvalho R J F, Evans R, Hoyle D C and Henderson J R 1994 *J. Phys.: Condens. Matter* **6** 9275–94